# Simulating diluted bitumen spills in boreal lake limnocorrals- Part 2: Factors affecting the physical characteristics and submergence of diluted bitumen

Stoyanovich, S.S[a]., Rodriguez-Gil, JR[b]., Hanson, M[c]., Hollebone, B.P[d]., Orihel, D. M[e]., Palace, V[b]., Faragher, R[d]., Mirnaghi, F.S[d]., Shah, K[d]., Yang, Z[d]., Blais, J.M[a*]

[a] Department of Biology, University of Ottawa, Ottawa, Ontario, K1N 6N5, Canada

[b] International Institute for Sustainable Development - Experimental Lakes Area, 111 Lombard Avenue, Suite 325, Winnipeg, Manitoba R3N 0T4, Canada

[c] Department of Environment and Geography, University of Manitoba, Winnipeg, MB, R3T 2N2, Canada.

[d] Emergencies Science and Technology Section, Environment and Climate Change Canada, Ottawa, Ontario, Canada

[e] Department of Biology and School of Environmental Studies, Queen's University, Kingston, ON K7L 3N6

*Corresponding Author:

Jules M. Blais
Department of Biology
University of Ottawa
20 Marie-Curie Ottawa, ON, Canada K1N 6N5
Tel: +1 (613) 562-5800 ext. 6650
Email: jules.blais@uottawa.ca

# Supporting Information

21 pages

3 Tables

15 Figures

# Supporting Methods

### 1.0 Set Up and Sampling

See Shah et al., (2019) for an in-depth overview of the design and execution of the controlled dilbit spills. This study was carried out at the International Institute for Sustainable Development Experimental Lakes Area (IISD-ELA), a unique research station in northwestern Ontario, Canada, dedicated to holistic, interdisciplinary field research and ecosystem manipulation studies.

*1.1 Dilbit Slick Sampling*

Subsamples of oil for chemical analysis were collected from the surface slick in each limnocorral using Teflon strips following ASTM Methods D4489 and D3325 (2013; 2017). The Teflon strip was passed through the oil slick until a sample approximately 2 – 5 mL had adhered. Oil samples for physical property analysis were collected using a pre-cleaned stainless-steel spoon which was passed through the dilbit slick until approximately 50 mL of sample was collected. Both types of samples were then placed in a certified 125mL wide mouth amber glass jars with lids lined with a TFE-fluorocarbon polymer film and sealed it. In the case of the control limnocorrals, we simply passed the wipe through the water surface. We placed samples immediately in a cooler and stored them away from any potential light sources to prevent further photochemical reactions.

## 2.0 Analytical Methods

*2.1 Sample Preparation*

Prior to use, we rinsed all glassware with acetone, dichloromethane (DCM) and hexane. Teflon strips were ultrasonicated with DCM for three times, dried at ambient temperature. The analysis of the concentrated solvent blank demonstrated the glassware and Teflon strips were clean and target-analyte free.

To extract collected oil samples, Teflon strips spiked with appropriate surrogates (o-terphenyl, $d_{50}$-tetracosane, $d_8$-naphthalene, $d_{10}$-acenaphthene, $d_{10}$-phenanthrene, $d_{12}$-benz[a]anthracene, and $d_{12}$-perylene) were ultrasonicated with DCM for 10 minutes, then the extracts were passed through sodium sulfate to get rid of water residues. Teflon strips were further rinsed with DCM until they are color free. The final extracts were diluted to 10 mL with DCM. Total solvent extractable materials (TSEM) were measured by gravimetric method by drying one-mL of above extracts to estimate the appropriate amount of extracts used for column clean-up. Appropriate amount of DCM extracts were solvent exchanged to hexane, and then quantitatively transferred onto a chromatographic column packed with 3 g of silica gel, which was topped with about 1 cm of anhydrous granular sodium sulfate and had been pre-conditioned with 20 mL of hexane, for sample cleanup and fractionation.

Hexane and a hexane-DCM mixture (1:1, v:v) were used to sequentially elute the saturated and aromatic compounds, respectively. These two fractions were concentrated under a gentle stream of nitrogen to appropriate volumes, spiked with internal standards (IS) (including 5-α-androstane for total (GC-detectable) petroleum hydrocarbons (TPHs) and alkanes, $C_{30}$ 17β(H),21β(H)-hopane for petroleum biomarker compounds and $d_{14}$-terphenyl , for polycyclic aromatic compound (PACs) analysis, respectively), and then adjusted to a volume of 1.0 mL for GC-MS and GC-FID analyses.

The saturated fraction was used for analysis of aliphatics (total saturated hydrocarbons, TSHs), *n*-alkanes, and biomarker terpanes and steranes; the aromatic fraction was used for analysis of aromatic hydrocarbons (TAHs), alkylated homologous PACs and other unsubstituted PACs.

*2.2 Instrument and Sample Analysis*

We determined TPH concentration (largely *n*-$C_9$ through *n*-$C_{40}$) on an Agilent 7890A gas chromatograph equipped with a flame ionization detector (FID) using Agilent OpenLAB ChemStation for data collection. We performed chemical separation usinga DB-5HT fused silica column (30 m × 0.25 mm i.d., 0.10 μm film thickness) and

hydrogen (1.3 mL/min) as a carrier gas. The injector and detector temperatures were 290°C and 300°C, respectively. The temperature program used for TPH determination was: 40°C for 2 min, ramp at 20°C/min to 340°C, and held for 20 min.

We analyzed target petroleum biomarker compounds using an Agilent 7890A GC equipped with an Agilent 5975C mass selective detector (MSD). The GC separation employed a DB-5MS capillary column (30 m × 0.25 mm i.d. × 0.25 μm film thickness). Samples (1.0 μL) injected into the GC in splitless mode (injector temperature at 290°C) with 1.0 mL/min of helium as carrier gas. The MSD operated in select ion monitoring (SIM) mode. The column temperature was held at 60°C for 2.0 min, and then programmed 6°C/min to 300 °C and held for 20 min. Data was acquired and analyzed with Agilent Enhanced MSD ChemStation. Recoveries of *o*-terphenyl and $d_{50}$-tetracosane, surrogates for GC-FID analysis of TPH, were determined to be 90 ± 9% and 94 ± 9% for all the oil samples.

## 3.0 Hyperbolic density and viscosity modelling:

The following model has been previously described by King et al., (2014; 2017) to describe changes in density and viscosity of surface oil samples (note density- $\rho$ can be interchanged with viscosity- $\nu$):

$$\rho = \rho_0 + (\rho_f - \rho_0)\left(\frac{t}{T+t}\right)^n \quad (2)$$

Using density as an example, $\rho_0$ and $\rho_f$ are the initial and final densities, T is a time constant representing the time to reach the plateau, and *n* is the rate at which $\rho_0$ approaches $\rho_f$, and t is time. The same approach can be used for viscosity measurements.

## Supporting Tables and Figures

**Table S1.** Physical Properties of fresh, unweathered CLWB

| Measurement | Mean ± SD (n =3) |
|---|---|
| Density at 15°C (g $mL^{-1}$) | 0.9215 ± 0.0003 |
| Density at 0 °C (g $mL^{-1}$) | 0.932 ± 0 |
| API Gravity | 21.5 |
| Viscosity at 15 °C (mPa·S) | 181 ± 0.2 |
| Viscosity at 0 °C (mPa·S) | 547 ± 0.5 |
| Flash Point (°C) | -6 ± 0 |
| Pour Point (°C) | -43 ± 3 |
| Sulfur Content (%) | 3.3 ± 0.01 |

**Table S2.** Identified targets and abbreviations

| n-Alkanes | Biomarker compounds | | Alkylated PAHs | |
|---|---|---|---|---|
| *n*-$C_9$ | C21 tricyclic terpane | $C_{21}$terpane | $C_0$-Naphthalene | $C_0$-N |
| *n*-$C_{10}$ | C22 tricyclic terpane | $C_{22}$terpane | $C_1$-Naphthalenes | $C_1$-N |
| *n*-$C_{11}$ | C23 tricyclic terpane | $C_{23}$terpane | $C_2$-Naphthalenes | $C_2$-N |
| *n*-$C_{12}$ | C24 tricyclic terpane | $C_{24}$terpane | $C_3$-Naphthalenes | $C_3$-N |
| *n*-$C_{13}$ | 18$\alpha$(H),21β(H)-22,29,30-trinorhopane | $C_{27}$Ts | $C_4$-Naphthalenes | $C_4$-N |
| 2,6,10-trimethyldodecane (TMD) | 17$\alpha$(H),21β(H)-22,29,30-trinorhopane | $C_{27}$Tm | $C_0$-Phenanthrene/anthracene | $C_0$-P |
| *n*-$C_{14}$ | 17$\alpha$(H),21β(H)-30-norhopane | $C_{29}$αβ hopane | $C_1$-Phenanthrenes/anthracenes | $C_1$-P |
| *n*-$C_{15}$ | 17$\alpha$(H),21β(H)-hopane | $C_{30}$αβ hopane | $C_2$-Phenanthrenes/anthracenes | $C_2$-P |
| n-$C_{16}$ | 22*S*-17$\alpha$(H),21β(H)-30-homohopane | $C_{31}$(S) hopane | $C_3$-Phenanthrenes/anthracenes | $C_3$-P |
| 2,6,10-trimethylpentadecane (TMP) | 22*R*-17$\alpha$(H),21β(H)-30-homohopane | $C_{31}$(R) hopane | $C_4$-Phenanthrenes/anthracenes | $C_4$-P |
| n-$C_{17}$ | 22*S*-17$\alpha$(H),21β(H)-30,31-bishomohopane | $C_{32}$(S) hopane | $C_0$-Dibenzothiophene | $C_0$-D |
| Pristane | 22*R*-17$\alpha$(H),21β(H)-30,31-bishomohopane | $C_{32}$(R) hopane | $C_1$-Dibenzothiophenes | $C_1$-D |
| n-$C_{18}$ | 22*S*-17$\alpha$(H),21β(H)-30,31,32-trishomohopane | $C_{33}$(S) hopane | $C_2$-Dibenzothiophenes | $C_2$-D |
| Phytane | 22*R*-17$\alpha$(H),21β(H)-30,31,32-trishomohopane | $C_{33}$(R) hopane | $C_3$-Dibenzothiophenes | $C_3$-D |
| n-$C_{19}$ | 22*S*-17$\alpha$(H),21β(H)-30,31,32,33-tetrakishomohopane | $C_{34}$(S) hopane | $C_0$-Fluorene | $C_0$-F |
| n-$C_{20}$ | 22*R*-17$\alpha$(H),21β(H)-30,31,32,33-tetrakishomohopane | $C_{34}$(R) hopane | $C_1$-Fluorenes | $C_1$-F |
| n-C21 | 22S-17$\alpha$(H),21β(H)-30,31,32,33,34-pentakishomohopane | $C_{35}$(S) hopane | $C_2$-Fluorenes | $C_2$-F |
| n-$C_{22}$ | 22*R*-17$\alpha$(H),21β(H)-30,31,32,33,34-pentakishomohopane | $C_{35}$(R) hopane | $C_3$-Fluorenes | $C_3$-F |
| n-$C_{23}$ | $C_{27}$ 20-5$\alpha$(H),14β(H),17β(H)-cholestane | $C_{27}$αββ sterane | $C_0$-Fluroanthene/pyrene | $C_0$-Fl |
| *n*-$C_{24}$ | $C_{28}$ 20-5$\alpha$(H),14β(H),17β(H)-ergostane | $C_{28}$αββ sterane | $C_1$-Fluroanthenes/pyrenes | $C_1$-Fl |
| *n*-$C_{25}$ | $C_{29}$ 20-5$\alpha$(H),14β(H),17β(H)-stigmastane | $C_{29}$αββ sterane | $C_2$-Fluroanthenes/pyrenes | $C_2$-Fl |
| *n*-$C_{26}$ | | | $C_3$-Fluroanthenes/pyrenes | $C_3$-Fl |
| *n*-$C_{27}$ | | | $C_4$-Fluroanthenes/pyrenes | $C_4$-Fl |
| *n*-$C_{28}$ | | | $C_0$-Benzonaphthothiophenes | $C_0$-B |
| *n*-$C_{29}$ | | | $C_1$-Benzonaphthothiophenes | $C_1$-B |
| *n*-$C_{30}$ | | | $C_2$-Benzonaphthothiophenes | $C_2$-B |
| *n*-$C_{31}$ | | | $C_3$-Benzonaphthothiophenes | $C_3$-B |
| *n*-$C_{32}$ | | | $C_4$-Benzonaphthothiophenes | $C_4$-B |
| *n*-$C_{33}$ | | | $C_0$-Chrysene | $C_0$-C |
| *n*-$C_{34}$ | | | $C_1$-Chrysenes | $C_1$-C |
| *n*-$C_{35}$ | | | $C_2$-Chrysenes | $C_2$-C |
| *n*-$C_{36}$ | | | $C_3$-Chrysenes | $C_3$-C |
| *n*-$C_{37}$ | | | Biphenyl | Bph |
| *n*-$C_{38}$ | | | Acenaphthylene | Acl |
| *n*-$C_{39}$ | | | Acenaphthene | Ace |
| *n*-$C_{40}$ | | | Anthracene | An |
| | | | Fluoranthene | Fl |
| | | | Pyrene | Py |
| | | | Benz(a)anthracene | BaA |
| | | | Benzo(b)fluoranthene | BbF |
| | | | Benzo(k)fluoranthene | BkF |
| | | | Benzo(e)pyrene | BeP |
| | | | Benzo(a)pyrene | BaP |
| | | | Perylene | Pe |
| | | | Indeno(1,2,3-cd)pyrene | IP |
| | | | Dibenzo(a,h)anthracene | DA |
| | | | Benzo(g,h,i)perylene | BgP |

**Table S3.** Chemical composition of fresh, unweathered 2018 CLWB. Full chemical names provided in Table S2.

| Aromatics | Conc. (µg/g) | *n*-Alkanes | Conc. (µg/g) | Biomarkers | Conc. (µg/g) | Metals[4] | Conc. (µg/g) |
|---|---|---|---|---|---|---|---|
| **ΣAromatics** | **7298** | **Σ*n*-alkanes** | **19260** | **ΣBiomarkers** | **1201** | Barium | 0.00 |
| **ΣParent & Alkyl PAHs** | **7220** | n-C9 | 2469 | C23 Terpane | 70.4 | Cadmium | 0.00 |
| ΣNAP C0 - C4 | 2154 | n-C10 | 2135 | C24 Terpane | 35.6 | Chromium | 0.00 |
| ΣPHE C0 - C4 | 1392 | n-C11 | 1585 | C27 Ts[3] | 17.6 | Iron | 3.66 |
| ΣDBT C0 - C3 | 1353 | n-C12 | 1525 | C27 Tm[4] | 61.6 | Molybdenum | 6.41 |
| ΣFLU C0 - C3 | 769 | n-C13 | 505 | C29αß Hopane | 146 | Nickel | 60.51 |
| ΣFLA C0 - C4 | 318 | TMD[1] | 1313 | C30αß Hopane | 178 | Titanium | 1.29 |
| ΣBNT C0 - C4 | 992 | n-C14 | 1258 | C31(S) Hopane | 32.1 | Vanadium | 137.2 |
| ΣCHR C0 - C3 | 241 | n-C15 | 978 | C31(R) Hopane | 80.0 | Zinc | 0.00 |
| **ΣEPA PAHs** | **77.8** | n-C16 | 781 | C32(S) Hopane | 54.8 | | |
| Biphenyl | 13.36 | TMP[2] | 485 | C32(R) Hopane | 50.4 | | |
| Acenaphthylene | 0.26 | n-C17 | 730 | C33(S) Hopane | 36.9 | | |
| Acenaphthene | 10.99 | Pristane | 377 | C33(R) Hopane | 38.3 | | |
| Anthracene | 3.59 | n-C18 | 608 | C34(S) Hopane | 25.4 | | |
| Fluoranthene | 4.94 | Phytane | 432 | C34(R) Hopane | 40.0 | | |
| Pyrene | 7.40 | n-C19 | 562 | C35(S) Hopane | 16.2 | | |
| Benz(a)anthracene | 5.58 | n-C20 | 490 | C35(R) Hopane | 34.4 | | |
| Benzo(b)fluoranthene | 5.42 | n-C21 | 453 | C27αßß Sterane | 30 | | |
| Benzo(k)fluoranthene | 1.45 | n-C22 | 400 | C28αßß Sterane | 122 | | |
| Benzo(e)pyrene | 5.83 | n-C23 | 356 | C29αßß Sterane | 104 | | |
| Benzo(a)pyrene | 3.57 | n-C24 | 313 | | | | |
| Perylene | 9.28 | n-C25 | 281 | | | | |
| Indeno(1,2,3-cd)pyrene | 2.14 | n-C26 | 257 | | | | |
| Dibenzo(ah)anthracene | 0.84 | n-C27 | 206 | | | | |
| Benzo(ghi)perylene | 3.11 | n-C28 | 156 | | | | |
| **ΣBTEX** | **10948** | n-C29 | 133 | | | | |
| Benzene | 1469 | n-C30 | 128 | | | | |
| Toluene | 4146 | n-C31 | 99.0 | | | | |
| Ethylbenzene | 410 | n-C32 | 66.0 | | | | |
| Xylenes | 4924 | n-C33 | 47.8 | | | | |
| | | n-C34 | 34.4 | | | | |
| | | n-C35 | 28.3 | | | | |
| | | n-C36 | 21.4 | | | | |
| | | n-C37 | 14.1 | | | | |
| | | n-C38 | 13.2 | | | | |
| | | n-C39 | 12.3 | | | | |
| | | n-C40 | 7.54 | | | | |

C0 are parent unsubstituted PAHs and C1 – C4 are alkylated PAHs.[1]TMD represents trimethyldecane and [2]TMP represents trimethylpentane. [3]*Ts* represents 18α(H) 22,29,30 trisnorphopane and [4]*Tm* represents 17α(H) 22,29,30 trisnorhopane. [4]Metal analysis on the source oil was performed via ASTM method D7111 with a detection limit of 0.1 µg/g


**Figure S1.** The addition of 180 L of CLWB (1:590 oil:water, v/v) onto the water surface of the limnocorral. (A) Overview of addition method, (B) View of telescopic arm and pumping system being held at approximately 5 – 10 cm from the water's surface. The oil exited the hose parallel to the waters surface to avoid forcing oil below the water surface and allowing it to spread out during the addition.

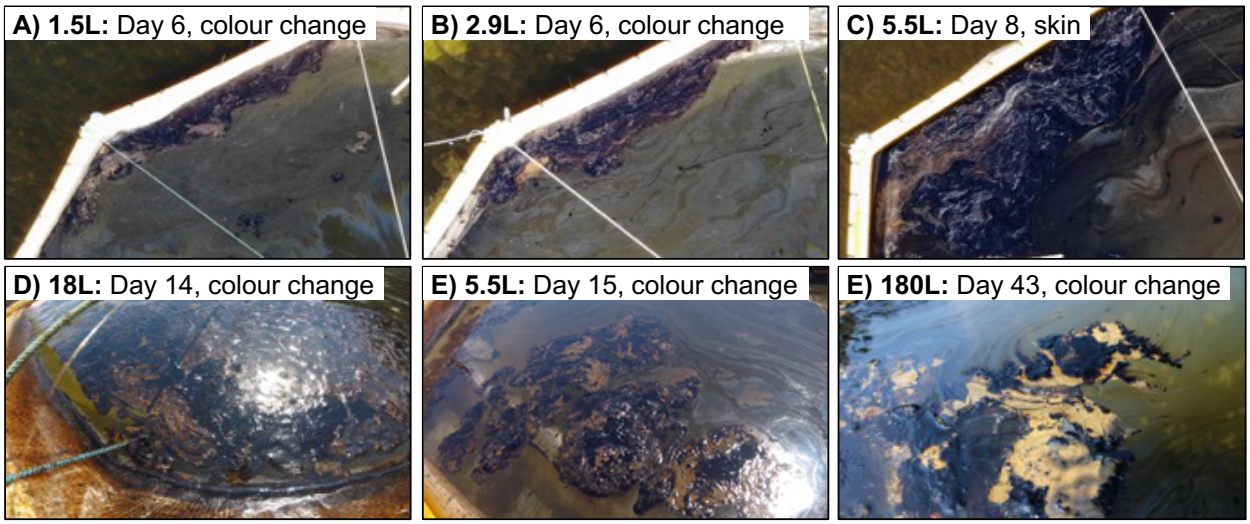


**Figure S2.** Examples of colour change and skin formation observed throughout the experiment.

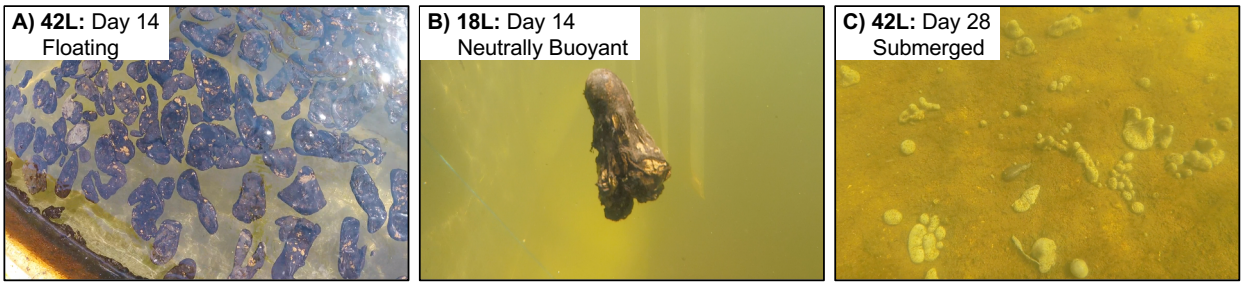


**Figure S3.** Examples of tar balls observed floating on the water surface (A), neutrally buoyant in the water column (B), and submerged on the sediments (C)

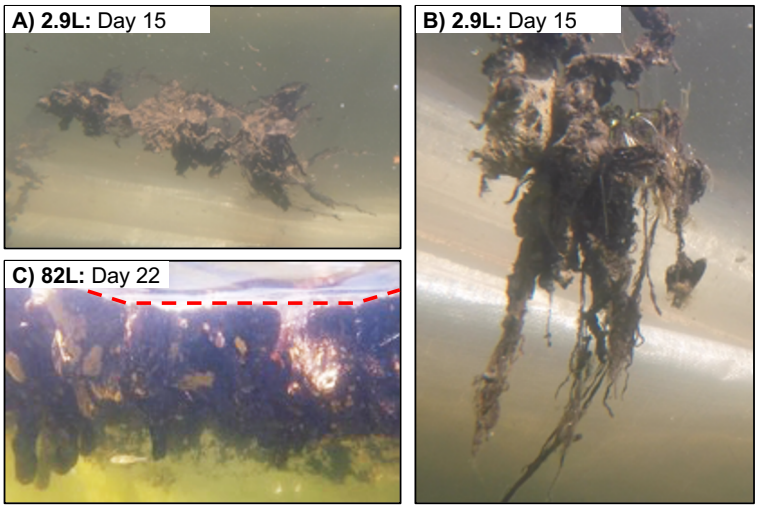


**Figure S4.** Changes in thickness of slick and formation of strings, water level represented by red dashed line in (C).

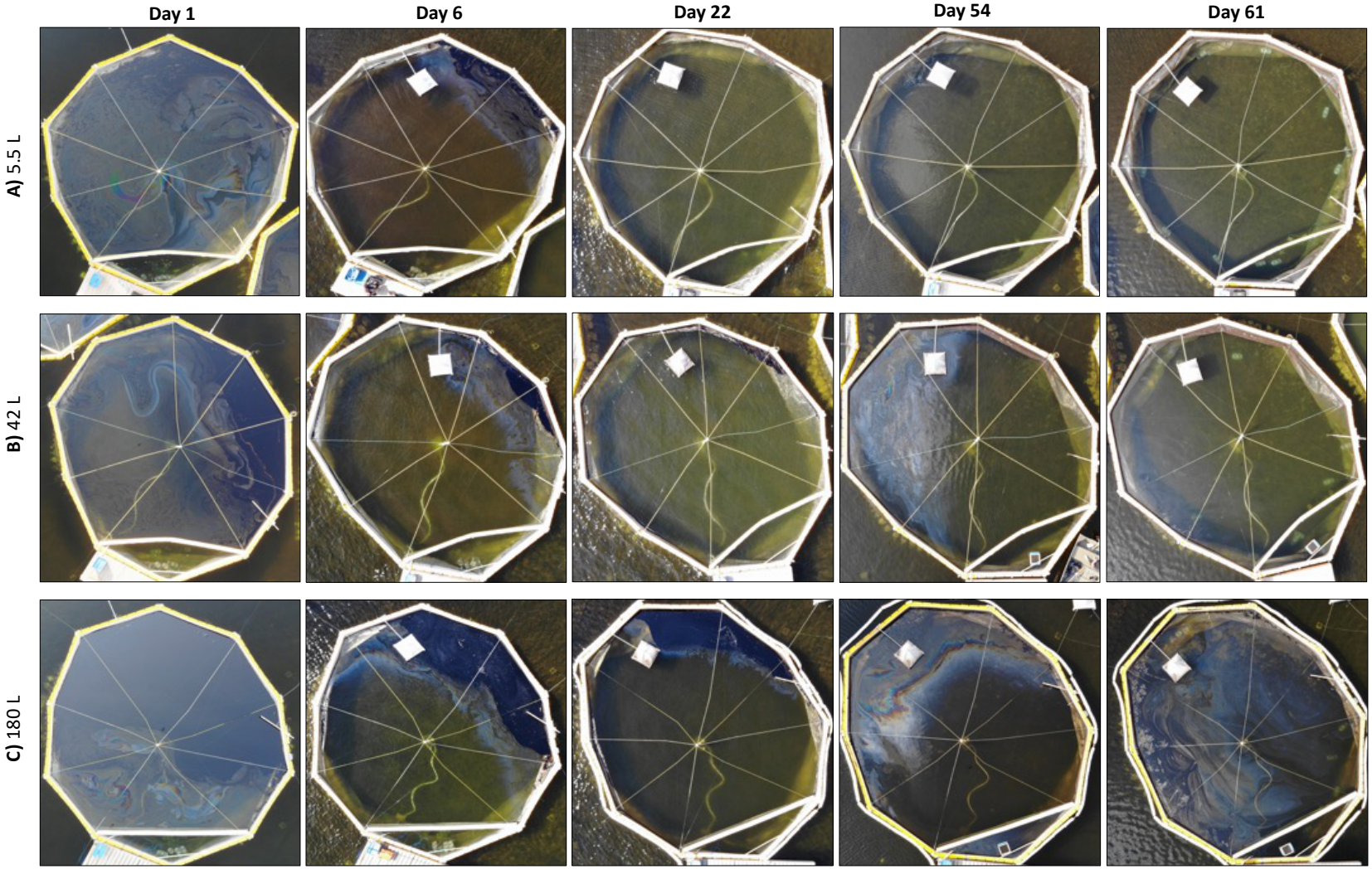


**Figure S5.** Aerial photograph timelines for a low (A), medium (B), and high (C) treatment showing changes in slick coverage and eventual disappearance.

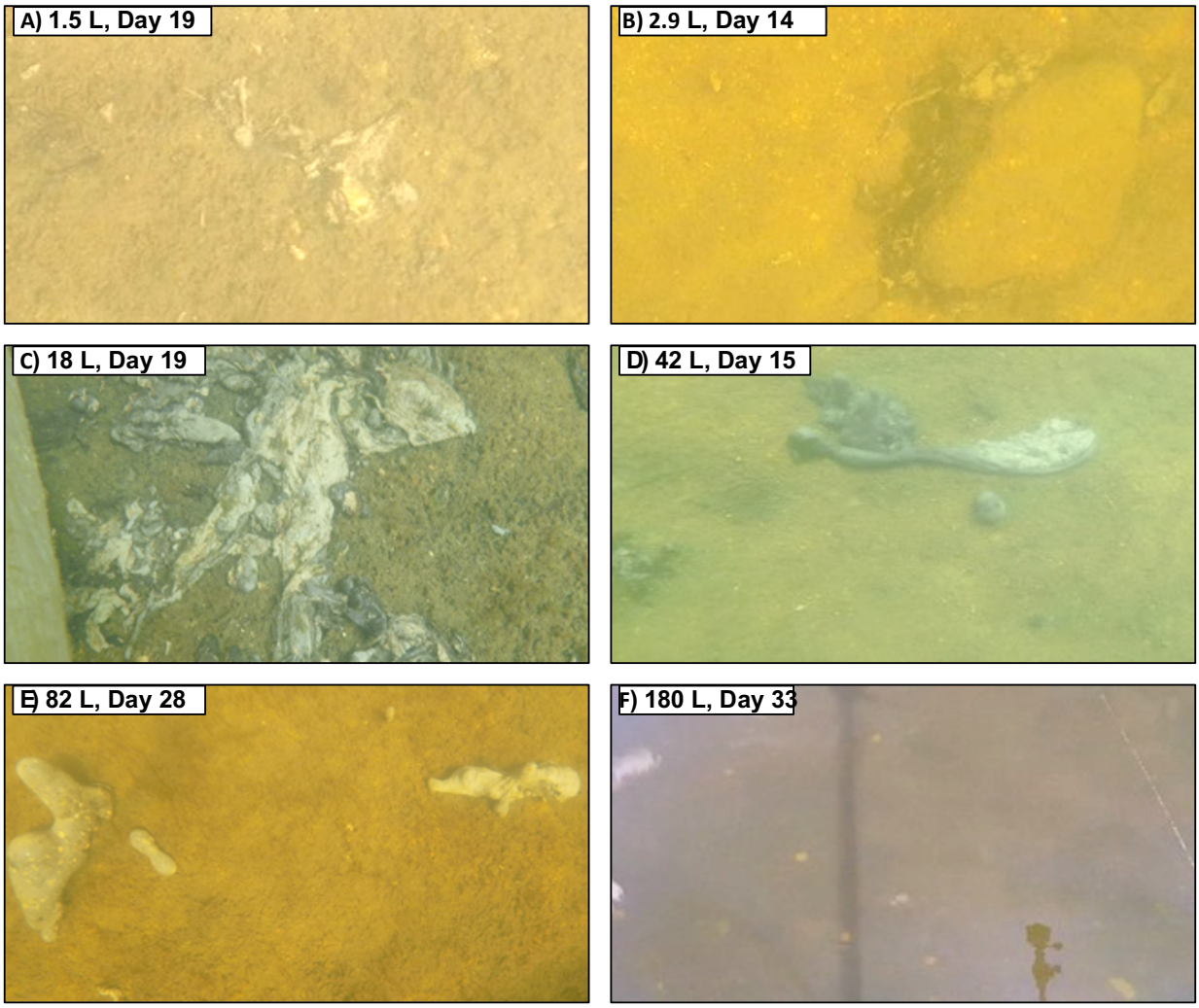


**Figure S6.** Examples of dilbit submergence in selected treatments early on in the experiment. All photographs were taken underwater directly above the sediment layer except for panel (F) which was taken above the water surface, the small white globules are dilbit lying on the sediments. While tarballs appear white in colour, this is an effect of the water column on the lighting, the tarballs appeared light to dark brown when removed from the water.

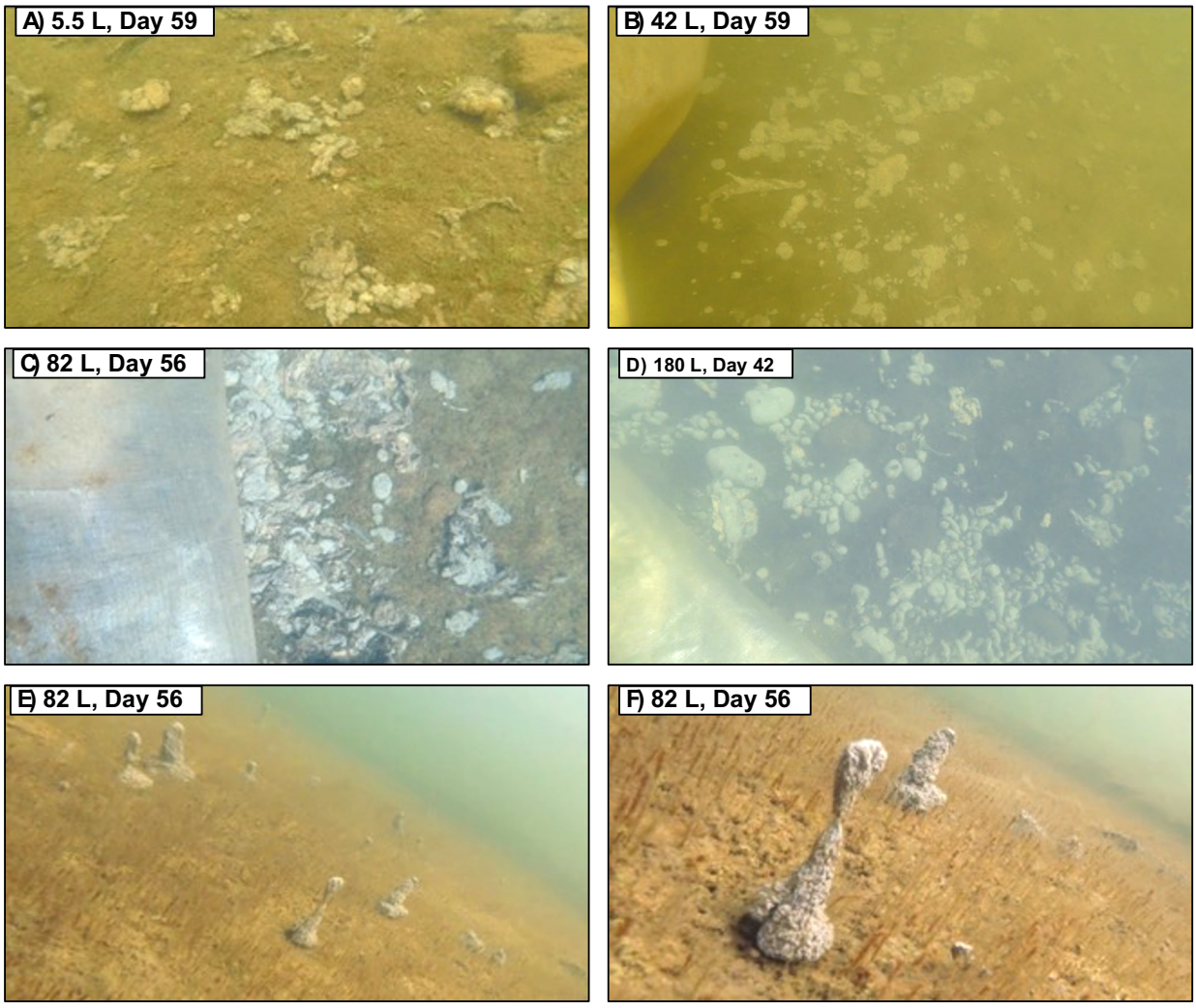


**Figure S7.** Examples of dilbit submergence in selected treatments later on in the experiment. All photographs were taken underwater directly above the sediment layer. Panels E) and F) depict the unique behaviour of tarballs that was observed only in the two highest treatments. Sections of the tarballs appear to be extending upward while being held down by the bulk oil suggesting that there may be density differences across the tarballs. While tarballs appear white in colour, this is an effect of the water column on the lighting, the tarballs appeared light to dark brown when removed from the water.

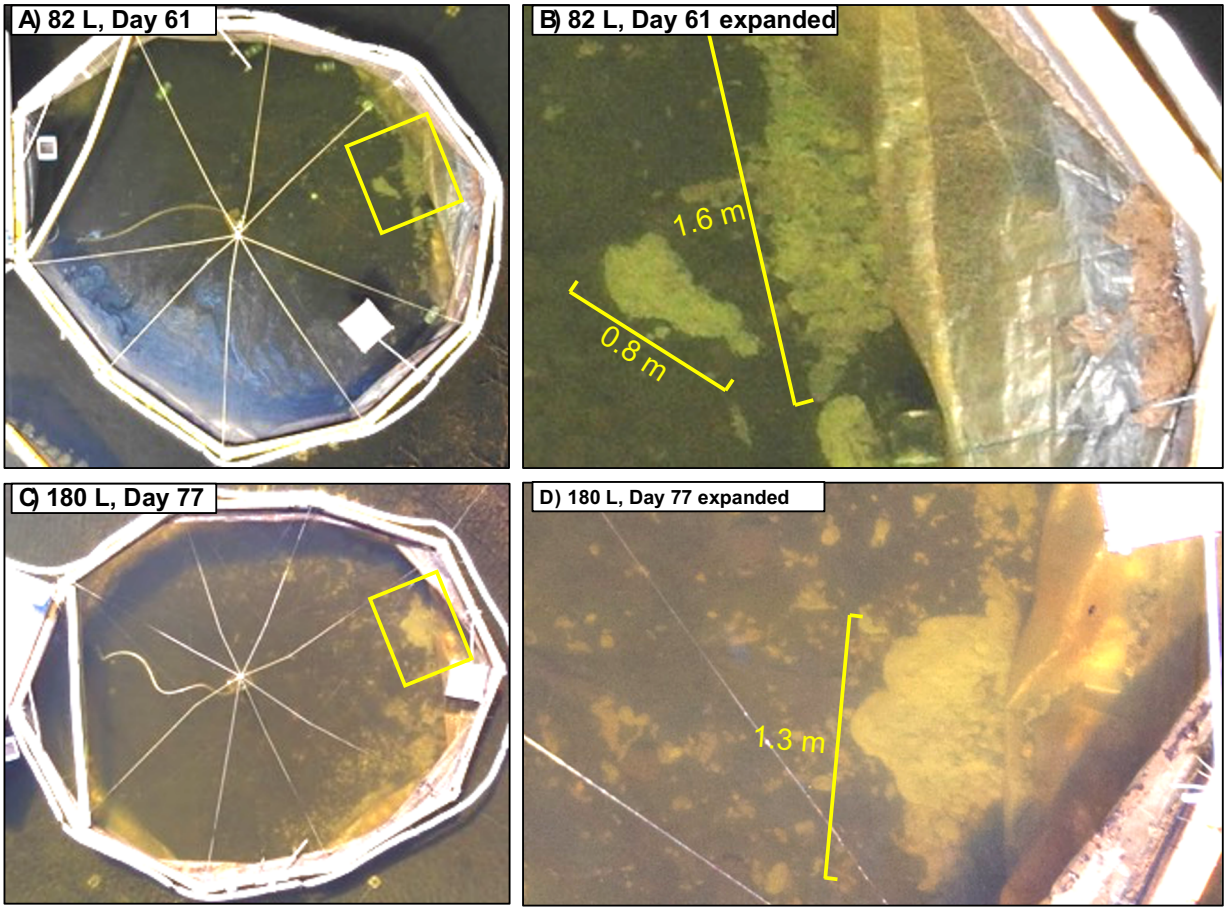


**Figure S8.** Examples of tar mats on the sediment bottom of the two highest treatments towards the end of the experiments. Panels B and C are zoomed in versions of the aerial photographs A and C. Tar mat measurements were made using ImageJ software version 1.50.

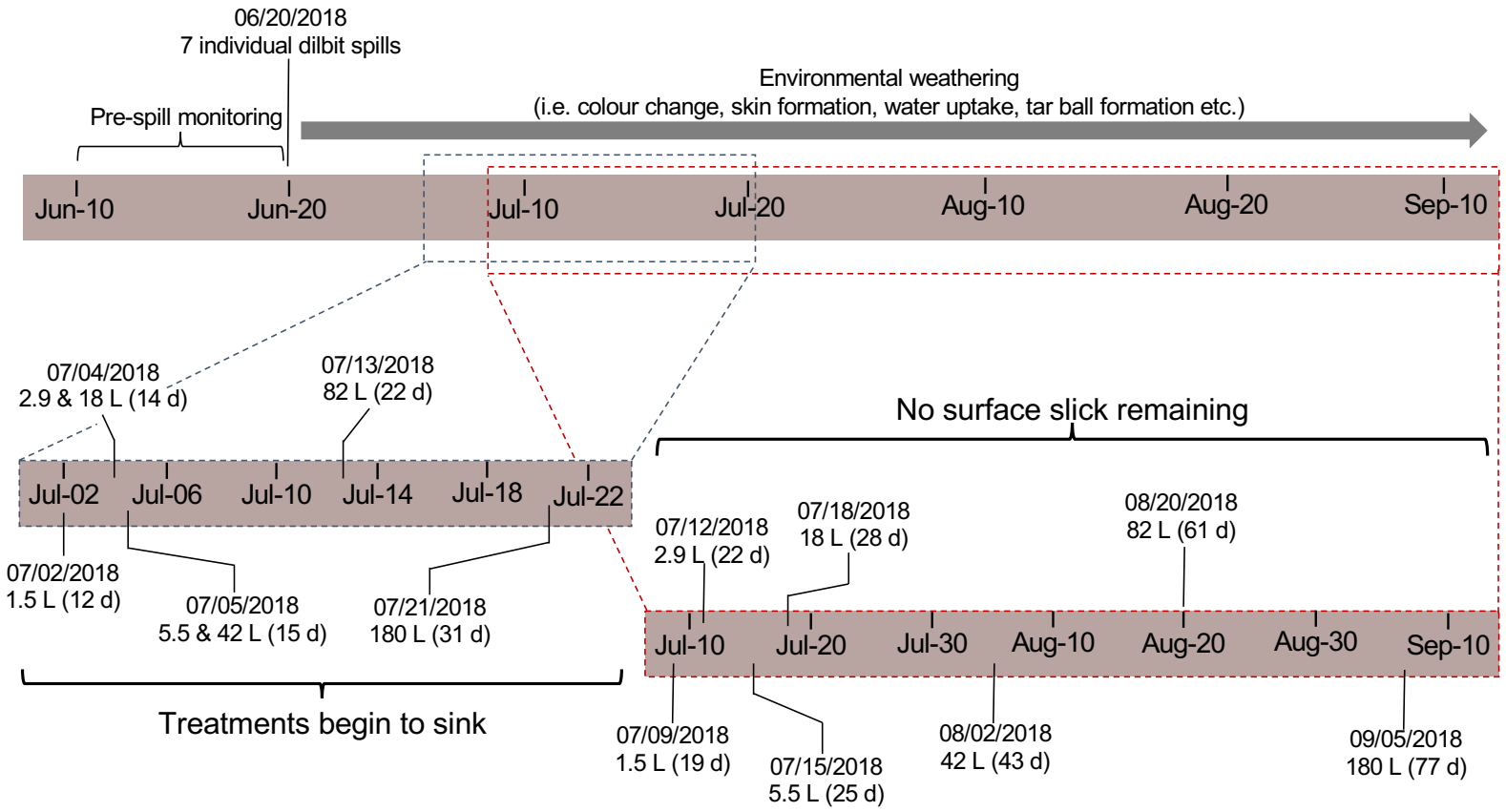


**Figure S9.** Detailed submergence timelines for each of the seven dilbit amended treatments during the summer of 2018.

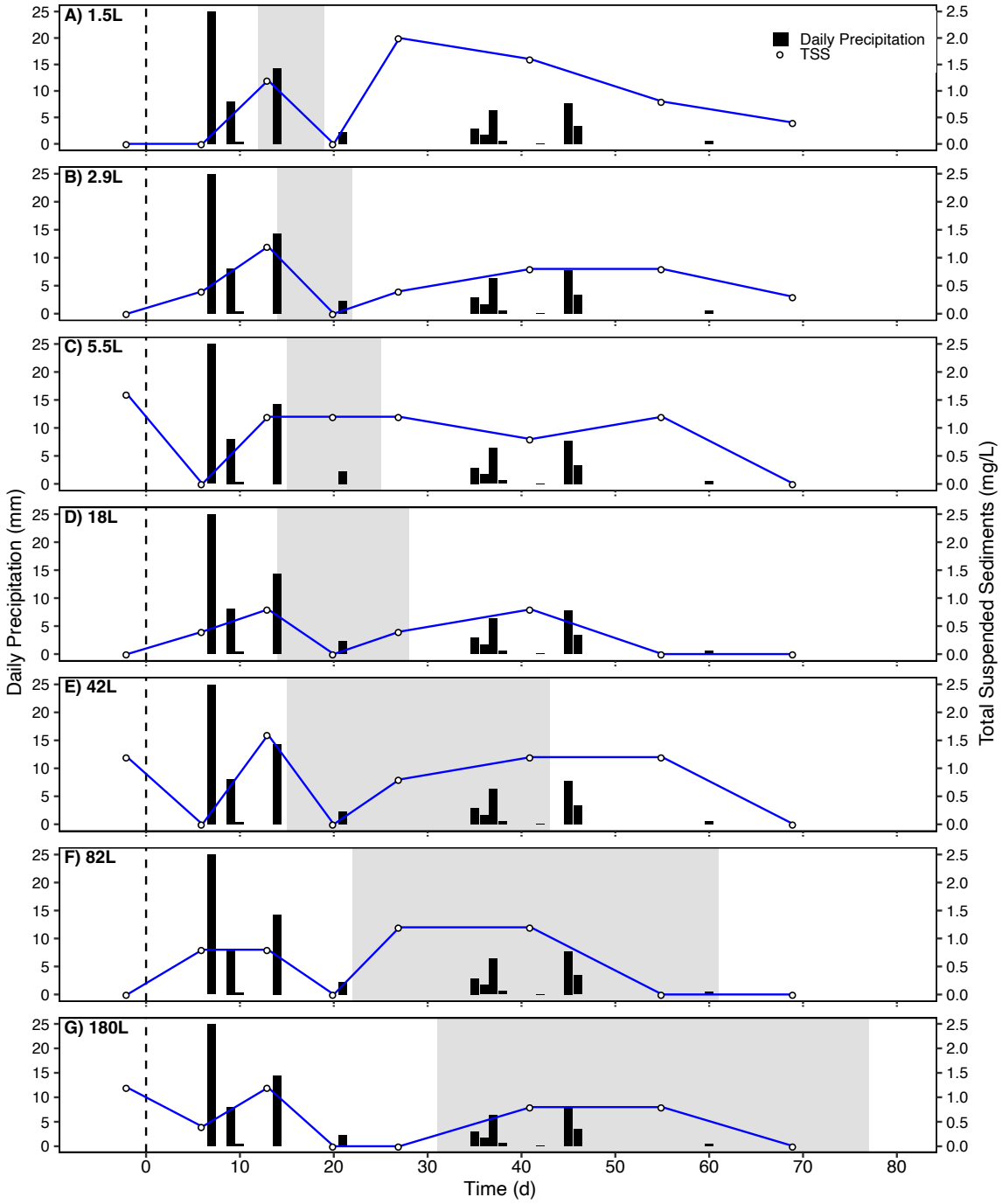


**Figure S10.** Monitoring of daily precipitation (black bars) and total suspended solids (open circles) over time in each of the dilbit treatments. Gray rectangles mark the onset and completion of submergence.

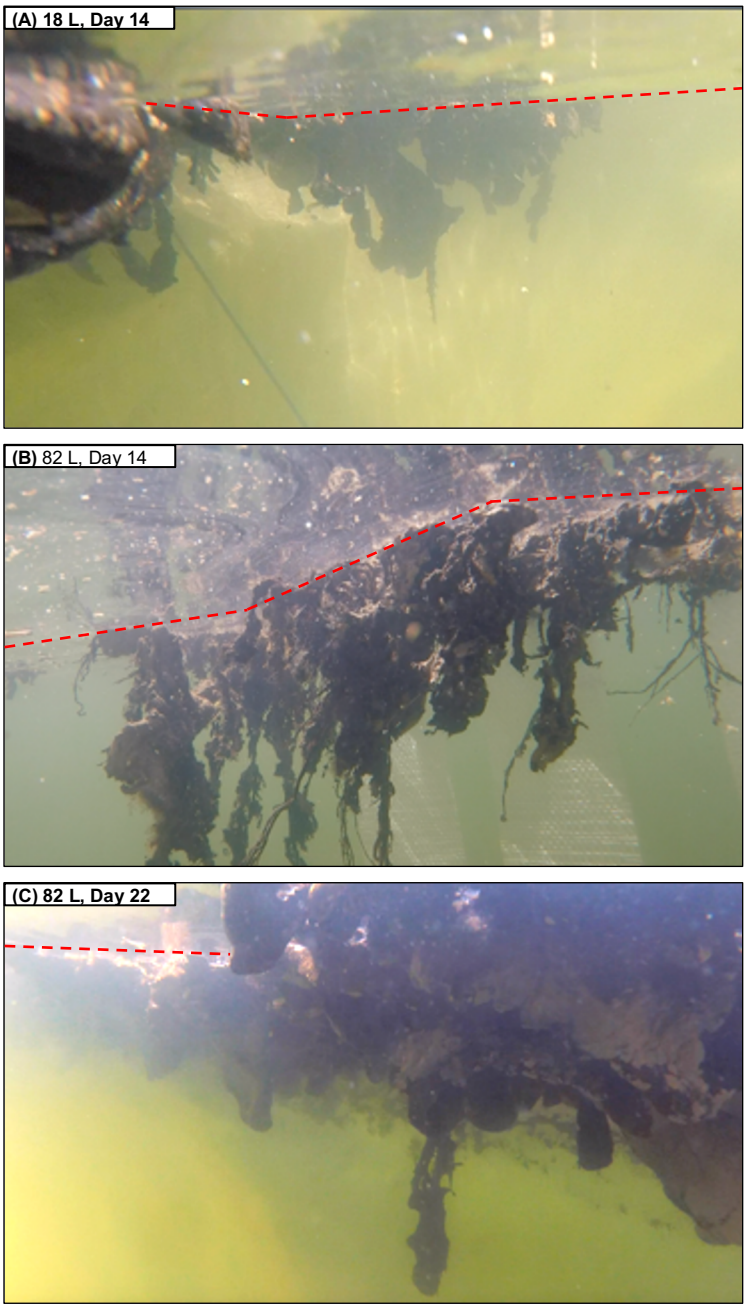


**Figure S11.** Photographs of floating slicks showing examples of sections of slick that are extending down into the water column while still remaining attached to the bulk surface slick. The red dashed lines represent the location of the water's surface for reference. With sufficient precipitation energy, it is possible that these slicks would break up, thus allowing the sinking sections to fully submerge to the sediments.

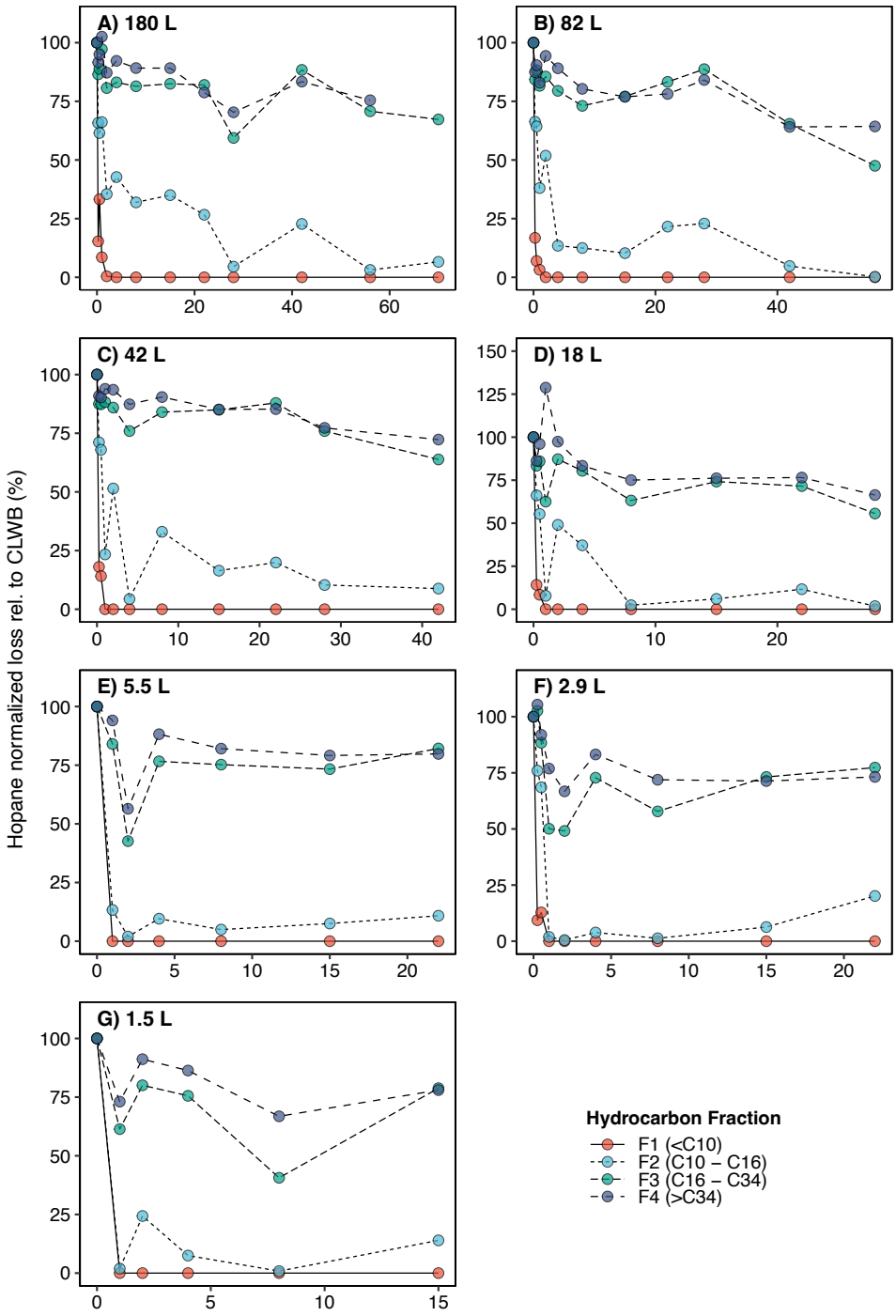


**Figure S12.** Temporal changes of the four petroleum hydrocarbon fractions separated by GC-FID in dilbit slicks samples. Concentrations were normalized to $C_{30}$ $\alpha\beta$ hopane and presented as percentage loss relative to the source CLWB dilbit. The varying x axis scale reflects when the respective dilbit slick was completely submerged, leaving no residual surface oil to sample. F3 and F4 fractions from panel G on day 8 and 15 were omitted due to analytical issues.

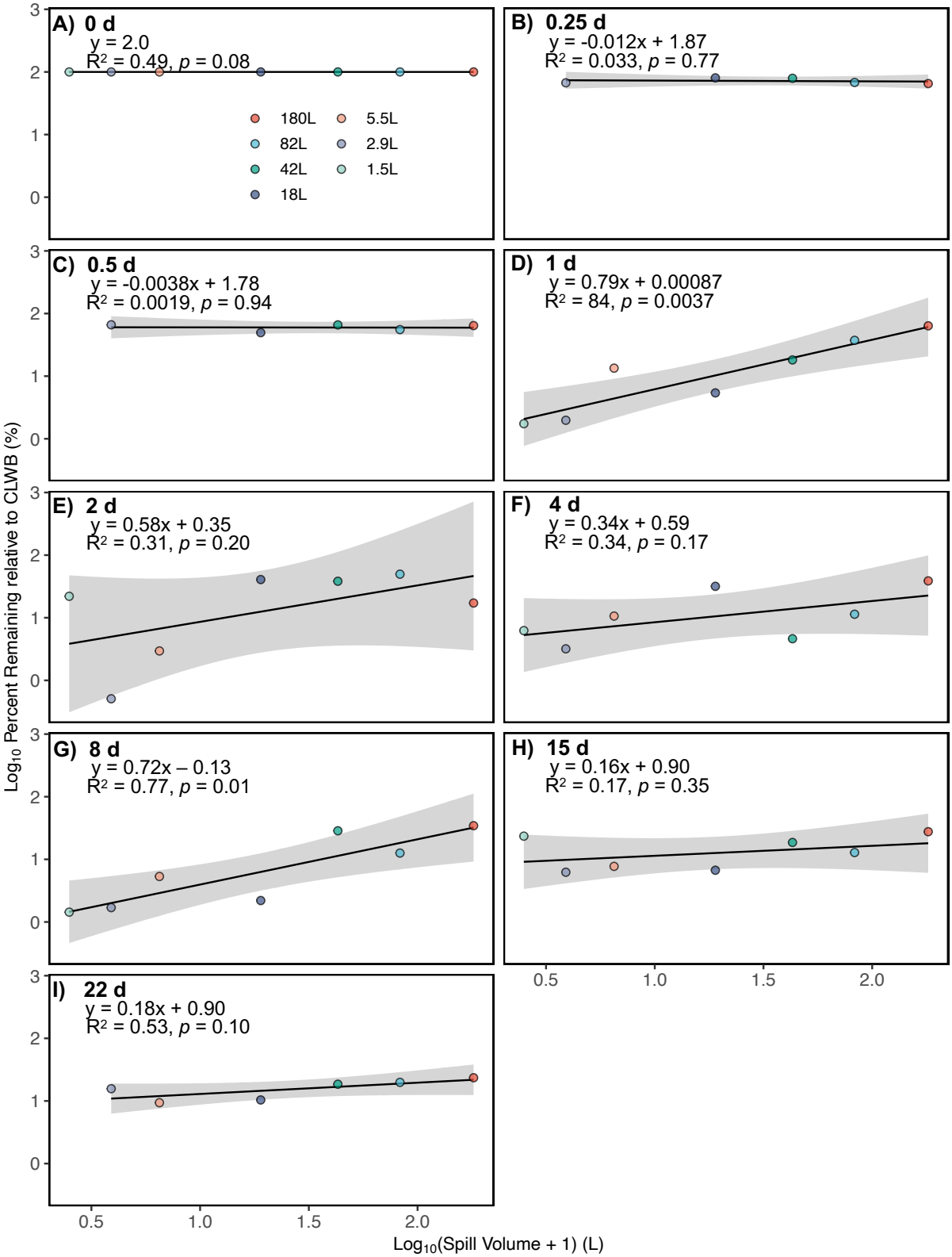


**Figure S13.** Individual regressions performed on slick samples collected at each time point. Data used to generate figure 4B in main research article. Each panel represents a sampling timepoint.

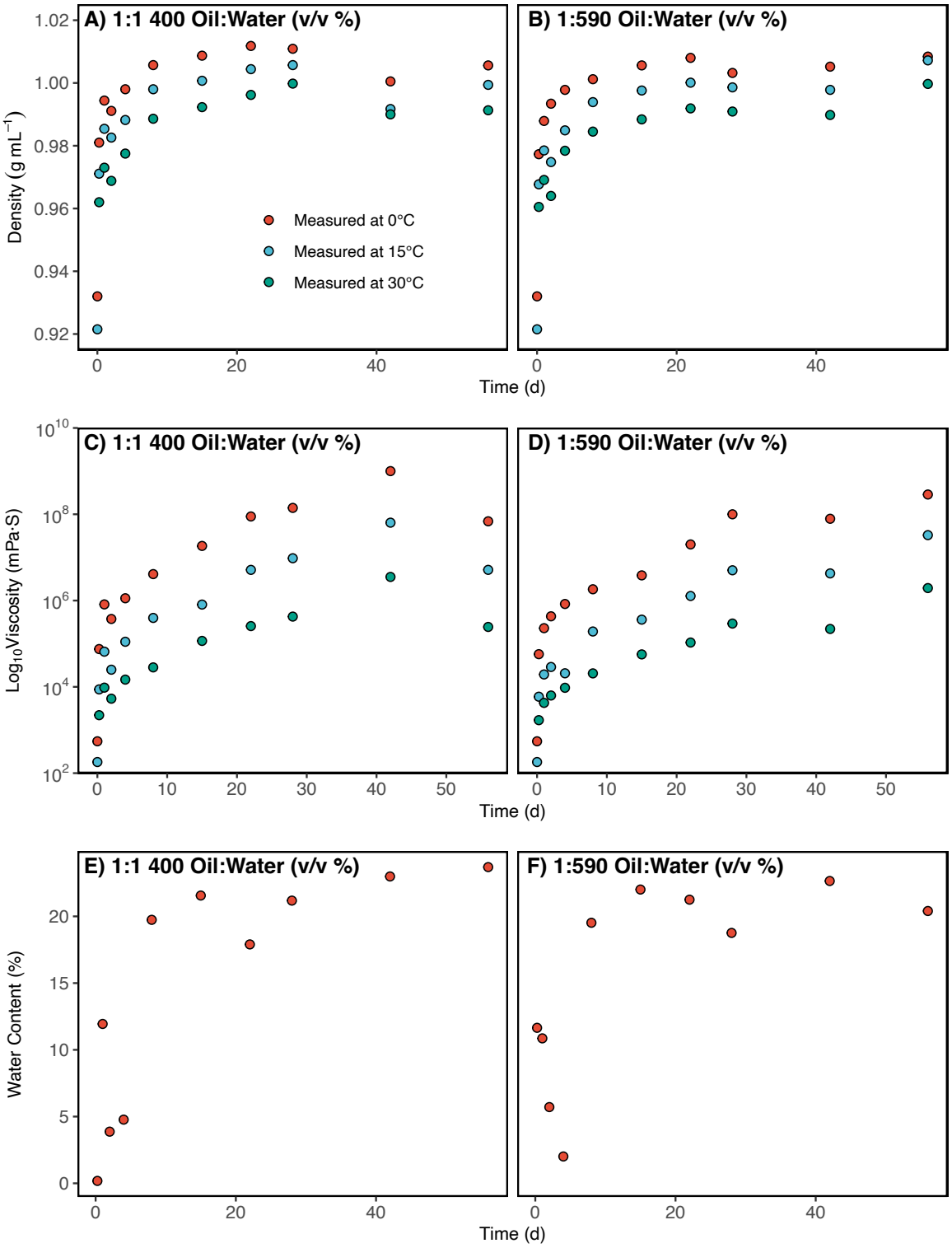


**Figure S14.** Temporal changes in physical properties (AB- density, CD- viscosity, EF- water content). Density and viscosity were measured at three different temperatures (0, 15, and 30 ºC), whereas water content was measured at room temperature.

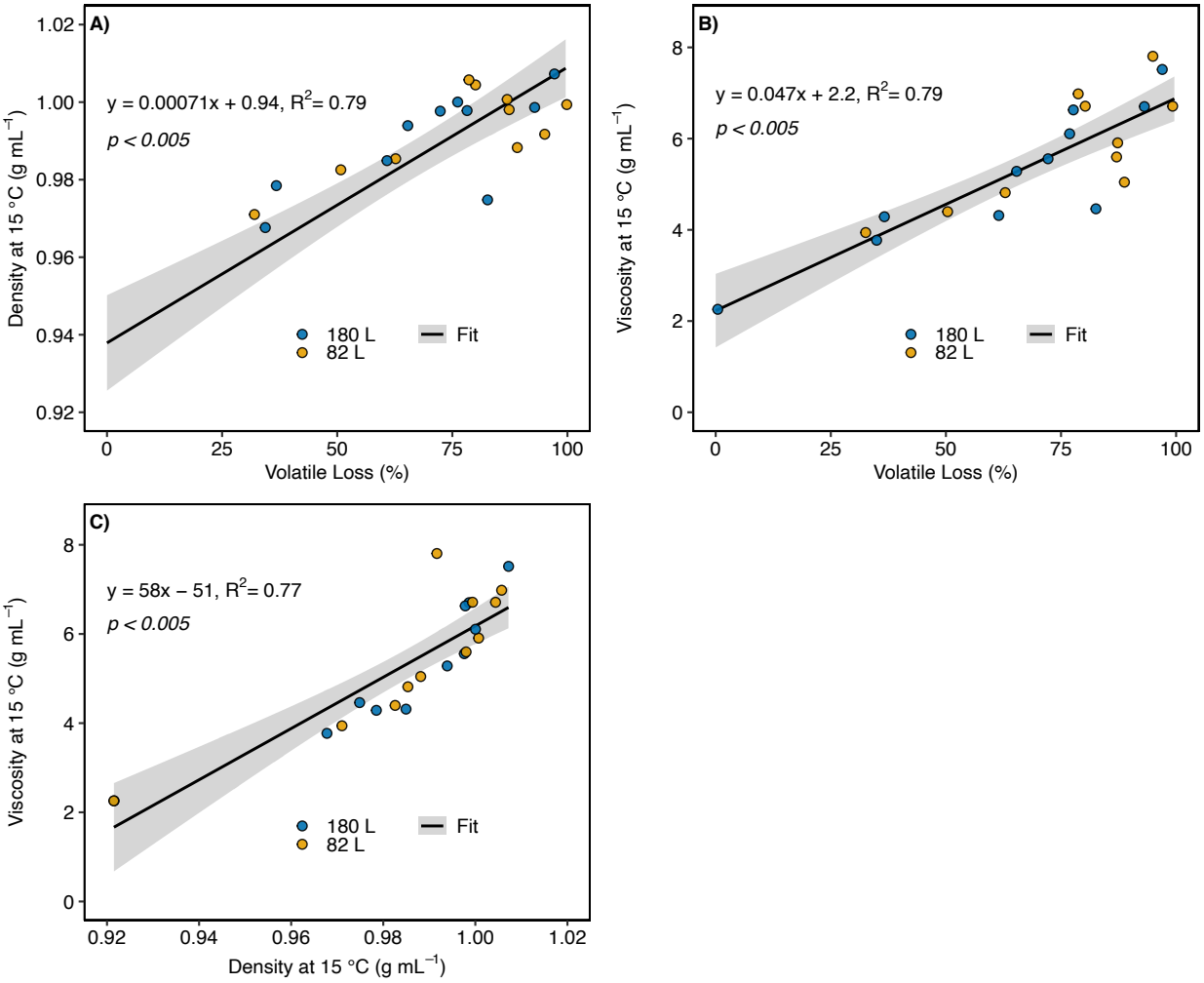


**Figure S15.** The relationship between (A) density measured at 15 ºC, (B) viscosity measured at 15 ºC, and the percentage of volatile hydrocarbon (<$C_{16}$) loss relative to the source CLWB. (C) The relationship between viscosity measured at 15 ºC and density measured at 15 ºC. Lines represent a fitted linear regression model and associated standard error.

**References**

ASTM D3325-90 Standard Practice for Preservation of Waterborne Oil Samples. 2013. ASTM Int. doi:10.1520/D3325-90R13.

ASTM D4489-95 Standard Practices for Sampling of Waterborne Oils. 2017. ASTM Int. doi:10.1520/D4489-95R17.

Fingas M, Fieldhouse B. 2014. Water-in-oil emulsions: formation and prediction. Handb Oil Spill Sci Technol. 225. doi:http://dx.doi.org/10.14355/jpsr.2014.0301.04.

King TL, Robinson B, Boufadel M, Lee K. 2014. Flume tank studies to elucidate the fate and behavior of diluted bitumen spilled at sea. Mar Pollut Bull. 83(1):32–37. doi:10.1016/j.marpolbul.2014.04.042.

King TL, Robinson B, Cui F, Boufadel M, Lee K, Clyburne JA. 2017. An oil spill decision matrix in response to surface spills of various bitumen blends. Environ Sci Process Impacts. 19(7):928–938. doi:https://doi.org/10.1039/C7EM00118E.

Shah K, Watson K, Hollebone B, Yang Z, Lambert P, Faragher R, Aljawahari M, Dey D, Mirnaghi F, Stoyanovich S, et al. 2019. The BOREAL Project: The Design and Execution of a Controlled Oil Spill Study in a Canadian Freshwater Lake. In: Proceedings of the Forty-second AMOP Technical Seminar. Environment and Climate Change Canada, Ottawa, ON, Canada. p. 276–294.

Yarranton H, Motahhari HR, Schoeggl F, Zhou JZ. 2015. Evaporative Weathering of Diluted Bitumen Films. J Can Pet Technol. 54(04):223–244. doi:https://doi.org/10.2118/174557-PA.